Enhanced Photoactivity of Oxygen-Deficient Anatase TiO2 Sheets with Dominant {001} Facets

ARTICLE · JANUARY 2009

Source: OAI

8 AUTHORS, INCLUDING:

Gang Liu
Chinese Academy of Sciences
98 PUBLICATIONS **8,265** CITATIONS
SEE PROFILE

Hao-Feng Lu
Australian National University
16 PUBLICATIONS **239** CITATIONS
SEE PROFILE

Lianzhou Wang
University of Queensland
218 PUBLICATIONS **5,500** CITATIONS
SEE PROFILE

Hui-Ming Cheng
Shenyang National Laboratory for Material…
489 PUBLICATIONS **33,698** CITATIONS
SEE PROFILE

Enhanced Photoactivity of Oxygen-Deficient Anatase TiO_2 Sheets with Dominant {001} Facets

Gang Liu,[†,‡] Hua Gui Yang,[§] Xuewen Wang,[†] Lina Cheng,[‡] Haofeng Lu,[†] Lianzhou Wang,[‡] Gao Qing (Max) Lu,*[,‡] and Hui-Ming Cheng*[,†]

Shenyang National Laboratory for Materials Science, Institute of Metal Research, Chinese Academy of Sciences, 72 Wenhua Road, Shenyang 110016, People's Republic of China, ARC Centre of Excellence for Functional Nanomaterials, School of Engineering and Australian Institute of Bioengineering and Nanotechnology, The University of Queensland, Queensland 4072, Australia, and Key Laboratory for Ultrafine Materials of Ministry of Education, School of Materials Science and Engineering, East China University of Science and Technology, Shanghai 200237, China

Received: August 11, 2009; Revised Manuscript Received: November 10, 2009

Constructing photocatalytically favorable surface structure in synthesizing photocatalysts plays an important role in enhancing the photocatalytic activity of semiconductor photocatalysts. In this report, oxygen-deficient anatase TiO_2 sheets with dominant {001} facets were synthesized via a facile one-pot hydrothermal route with solid metallic titanium diboride as precursor. In contrast to anatase TiO_2 sheets with dominant {001} facets free of oxygen deficiency and surface fluorine, anatase TiO_2 sheets with oxygen deficiency and surface fluorine are subject to obvious surface reconstruction as evidenced by two new Raman-active modes at 155 and 171 cm^{-1} and the weakened B_{1g} mode at 397 cm^{-1}. Further analysis based on X-ray photoelectron spectroscopy (XPS) spectra of Pt 4f and F 1s provided a clear evidence for the greatly strengthened interaction between Pt-loaded and TiO_2 matrix as a result of a special electron-transfer process on the reconstructed surface structure of TiO_2 with both oxygen deficiency and fluorine. Importantly, the reconstructed surface structure as well as the strengthened interaction between Pt-loaded and TiO_2 matrix can substantially enhance the hydrogen evolution rate from photocatalytic water splitting reactions.

1. Introduction

Anatase TiO_2 as one of the most important functional metal oxides has been extensively investigated for its wide applications from catalysis to photoelectrochemistry.[1−6] Owing to the low atomic coordination numbers of exposed atoms and the wide bond angle of Ti−O−Ti, the anatase TiO_2 (001) facet is theoretically considered to be more reactive than the (101) facet in heterogeneous reactions.[7] But the (101) facet with much lower surface energy than (001) is usually evidenced as the majority in most synthetic anatase TiO_2 particles. In the recent work by Yang et al.,[8] high-quality truncated anatase bipyramids with a high percentage of 47% (001) facet was prepared using titanium fluoride (TiF_4) aqueous solution and hydrofluoric acid as the single crystal anatase's precursor and crystallographic controlling agent, respectively. Recently, this percentage was further improved up to 64% by employing an alternative solvothermal route.[9] In both cases, oxygen deficiency detected in the resultant surface fluorine terminated anatase single crystals is at a negligible level according to the results by X-ray photoelectron spectroscopy (XPS), Raman, and UV−vis absorption spectra. Meanwhile, several works have investigated other routes to prepare anatase TiO_2 sheets with desirable (001) facets.[10]

On the other hand, oxygen deficiency in anatase TiO_2 plays an important role in positively contributing to the reactivity of anatase TiO_2 for heterogeneous reactions. Nakamura et al.[11] reported both enhanced UV- and additional visible- photodegradation capability of NO over plasma-treated anatase TiO_2 with oxygen vacancies, and a similar favorable role of oxygen vacancies was also shown in $TiO_{1.8}$ thin film by Justicia et al.[12] This is because, besides the induced electronic structure modification, these existing oxygen deficiencies can act importantly as specific reaction sites for reactant molecules in heterogeneous reactions.[13] In the reported cases in terms of oxygen vacancies, anatase TiO_2 particles are enclosed with poorly defined facets or dominant (101) facet. Considering the merits of anatase (001) facet for heterogeneous reactions, it is therefore reasonable to expect that oxygen-deficient anatase TiO_2 with dominant (001) facet will be a desirable candidate for many attractive applications such as photocatalysis by creating more favorable surface structures (i.e., exposed surface atoms with lower coordinated numbers and/or related surface reconstructions).

Even though the synthetic strategies to prepare well-defined (001) facet dominant anatase TiO_2 single crystals were recently developed,[8,9] it is still challenging to impart oxygen deficiency into such highly crystalline TiO_2 under mild post-treatment conditions, while the post-treatment under extreme conditions can lead to undesirable changes including crystalline phase transformations. Herein, we report a facile and simple route to realize one-pot synthesis of oxygen-deficient anatase TiO_2 sheets with dominant (001) facets using solid metallic titanium diboride (TiB_2) as precursor, which has the merit of slow hydrolysis, nontoxic nature, and noncorrosive byproduct.[14] Furthermore, the photoactivity of oxygen-deficient anatase TiO_2 sheets in terms of the measured capability of hydrogen evolution under UV−vis

* To whom correspondence should be addressed. Fax: +61 7 33656074 (G.Q.L.); +86 24 23903126 (H.-M.C.). Tel.: + 61 7 33653735 (G.Q.L.); +86 24 23971611 (H.-M.C.). E-mail: maxlu@uq.edu.au (G.Q.L.); cheng@imr.ac.cn (H.-M.C.).
† Chinese Academy of Sciences.
‡ The University of Queensland.
§ East China University of Science and Technology.

10.1021/jp907749r
Published on Web 12/08/2009

irradiation is greatly enhanced compared to that of the anatase TiO_2 sheets free of oxygen deficiency. The reconstructed surface structure and resultant strengthened interaction between Pt-loaded and TiO_2 matrix shed light on developing efficient photocatalysts.

2. Experimental Section

2.1. Synthesis of Oxygen-Deficient Anatase TiO_2 Sheets. TiB_2 was employed as the TiO_2 precursor. In a typical synthesis procedure, TiB_2 powder precursor was suspended into 20 mL of aqueous solution of HF (0.5 to ~1.5 M), followed by hydrothermal treatment in a Teflon-lined autoclave with a volume of 100 mL at 180 °C for 12 h. After the reaction, the product was collected by centrifugation and washed with deionized water three times to remove dissoluble ionic impurities. Then the samples with a dark blue color were dried at room temperature for 12 h.

2.2. Removal of Oxygen Deficiency from Anatase TiO_2 Sheets. The powder sample of as-prepared oxygen-deficient anatase TiO_2 sheets was heated at 600 °C in static air atmosphere in a furnace for 2 h. Then, the sample was naturally cooled to room temperature.

2.3. Cocatalyst Loading. Pt loading was conducted by an impregnation method from an aqueous solution of $H_2PtCl_6 \cdot 6H_2O$. A sample of TiO_2 was added into aqueous solution containing a desirable amount of $H_2PtCl_6 \cdot 6H_2O$ (1 $mg \cdot mL^{-1}$ Pt) in an evaporating dish at 60 °C. The suspension was evaporated under constant stirring with a glass rod, and the resulting powder was collected and heated in air at 180 °C.

2.4. Characterization. X-ray diffraction patterns of samples were recorded on Rigaku diffractometer using Cu irradiation. Morphology and crystal structure were determined by scanning electron microscopy (SEM) and transmission electron microscopy (TEM) performed on JEOL (6300) and Tecnai F30 instruments. A UV−vis spectrophotometer (JASCO-V550) was used to obtain the optical absorbance spectra of the samples. Raman spectra were collected on LabRam HR 800. Chemical compositions of derived TiO_2 polymorphs were analyzed using XPS (Thermo Escalab 250, a monochromatic Al Kα X-ray source). All binding energies were referenced to the C 1s peak (284.6 eV) arising from adventitious carbon.

2.5. Photocatalytic Activity Tests. Water splitting reactions were carried out in a top-irradiation vessel connected to a glass closed gas circulation system. Photocatalyst powder was dispersed in 300 mL of water solution containing 10% methanol in volume. The reaction temperature was maintained between 4 and 9 °C. The light source was a 300 W Xe lamp. The amount of H_2 evolved was determined using gas chromatography (Agilent Technologies: 6890N). The detailed schematic of the water splitting measurement equipment can be found in ref 15.

3. Results and Discussion

In a typical synthesis procedure, 100 mM solid TiB_2 powder with a particle size of several micrometers in 1 M hydrofluoric acid (HF) was hydrothermally treated at 180 °C in a Teflon-lined stainless steel autoclave. The starting solid TiB_2 in black color is in hexagonal symmetry (*P6/mmm*) as characterized by alternating hexagonal layers of titanium and boron atoms.[14,16] The X-ray diffraction (XRD) intensity of TiB_2 (Figure 1b, Cu Kα radiation) is quite similar to the calculated value of the bulk TiB_2 crystals (Figure 1a), indicating that the crystalline TiB_2 used in our experiments is enclosed mainly by thermodynamically stable facets such as {110} and {001}. After hydrothermal treatment, anatase TiO_2 sheets (Figure 1c) are derived from TiB_2,

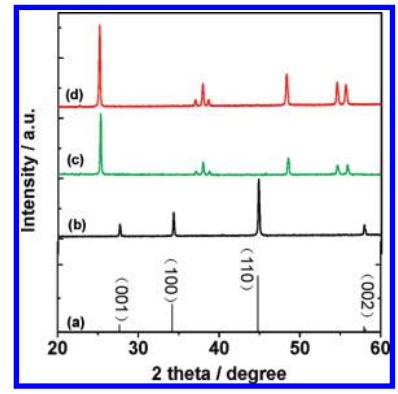

Figure 1. Calculated XRD pattern of bulk TiB_2 (ref 14) (a), XRD pattern of pristine TiB_2 (b), oxygen-deficient anatase TiO_2 sheets (c), and calcined anatase TiO_2 sheets at 600 °C in air for 2 h (d).

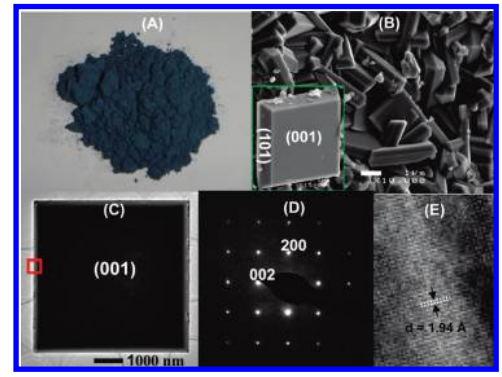

Figure 2. Optical photo (A), typical SEM and TEM images (B and C), SAED patterns (D), and high-resolution TEM image (E) of oxygen-deficient anatase TiO_2 sheets. The high-resolution TEM image was recorded in the rectangular area in panel C.

and interestingly, the as-prepared oxygen-deficient anatase TiO_2 sheets appear in a dark blue color (Figure 2A), which is strikingly different from the general white color of pure TiO_2 prepared by wet-chemistry routes. The SEM image of the representative anatase TiO_2 sheets is shown in Figure 2B. According to the symmetries of anatase TiO_2, the two flat and square surfaces in the well-faceted crystal structure of anatase TiO_2 sheets can be ascribed to (001) and the eight isosceles trapezoidal surfaces are {101} facets of the anatase TiO_2 single crystals.[8] The average size of the anatase TiO_2 sheets is ca. 4 μm with a thickness of ca. 1 μm and the percentage of ca. 56% (001) facet, which is comparable with the (001) facet percentage of the recently reported sheets using TiF_4 as precursor,[9] but 4 times larger in size and thickness. The single-crystal nature of the anatase TiO_2 sheets is further confirmed by typical TEM images and selected area electron diffraction (SAED) in Figure 2C−E. The high-resolution TEM image (Figure 2D) recorded on the rectangular area in Figure 2C gives continuous (200) atomic planes with a lattice spacing of 1.94 Å.

The optical absorption spectra of oxygen-deficient anatase TiO_2 sheets and anatase sheets free of oxygen deficiency are shown in Figure 3. Both anatase TiO_2 sheets have a nearly overlapped intrinsic absorption edge with the threshold of 393 nm. Derived from the plot of the Kubelka−Munk function versus the energy of the light absorbed (the inset in Figure 3) assuming titania as indirect semiconductor, the band gap of the obtained anatase TiO_2 sheets is 3.16 eV. In contrast to the previously synthesized anatase TiO_2 sheets,[8,9] an additional strong absorption band beyond 400 nm up to the infrared range appears in the as-prepared oxygen-deficient sheets. This absorption band is attributed to low-energy photon and/or thermal

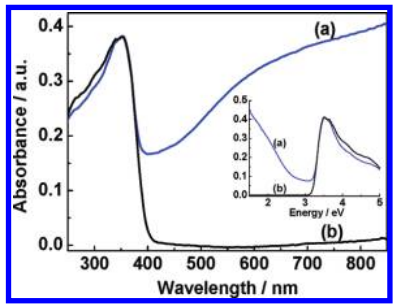

Figure 3. UV−vis absorption spectra of the oxygen-deficient anatase TiO_2 sheets (a) and anatase TiO_2 sheets free of oxygen deficiency by calcining at 600 °C in air (b). The inset is their corresponding plot of transformed Kubelka−Munk function vs the energy of the light absorbed.

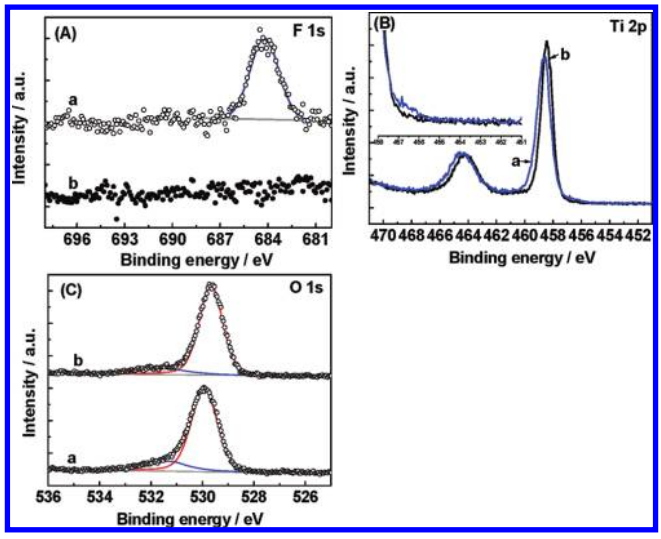

Figure 4. High-resolution XPS spectra of (A) F 1s, (B) Ti 2p, and (C) O 1s for (a) oxygen-deficient anatase TiO_2 sheets and (b) anatase TiO_2 sheets free of oxygen deficiency.

excitations of trapped electrons in localized states of defects (i.e., oxygen deficiency related Ti^{3+}) just below the conduction band minimum to the conduction band.[17] After calcination of anatase sheets in air, this absorption band disappears as shown in Figure 3b, further indicating the presence of oxygen vacancies in the anatase TiO_2 sheets.

To investigate the elemental compositions and the binding states of derived anatase TiO_2 sheets, high-resolution XPS was used to detect the surface B 1s, F 1s, Ti 2p, and O 1s core levels (Figure 4). No boron element was detected from the anatase TiO_2 sheets obtained. The as-prepared anatase TiO_2 sheets are rich in fluorine as surface $TiOF_2$ or Ti−F species,[8,18] and the binding energies of Ti $2p_{3/2}$ and O 1s are 458.6 and 530.0 eV, respectively. More importantly, a detectable shoulder appears in the low-energy range (457.5−455.5 eV) of the Ti 2p spectrum, which is attributed to Ti^{3+} in the TiO_2 sheets obtained. Regarding the origin of the Ti^{3+} defects in our fluorine-terminated anatase TiO_2 sheets, two possible mechanisms should be considered according to the literature.[19] One is that oxygen deficiency transfers its extra two electrons to the adjacent two Ti^{4+} atoms to form Ti^{3+}.[19a] The other is that the possible bulk substitutional F^- for lattice O^{2-} atoms can result in the localization of the extra one electron in a 3d orbital of Ti^{4+} and thus Ti^{3+}.[19b] The most obvious difference as a result of Ti^{3+} defects from the above two mechanisms lies in that the reported F-derived Ti^{3+} cannot cause any observed photon excitation in the infrared region,[19b] whereas oxygen deficiency related Ti^{3+} can result in such excitations[19a] due to the different energy levels of the Ti^{3+} state. Our Ti^{3+} contained TiO_2 shows an obvious photon excitation in the infrared region (see Figure 3), indicating that the Ti^{3+} detected is dominantly derived from oxygen deficiency. Upon the calcination of the oxygen-deficient anatase TiO_2 in air, two features are evident. One is the removal of surface fluorine, which is consistent with the previously reported result,[8] and the other is the disappearance of low-energy shoulder in the Ti 2p spectrum and peak shift of Ti $2p_{3/2}$ (from 458.6 to 458.4 eV) and O 1s (from 530.0 to 529.6 eV) toward low energy as a result of removing oxygen vacancies.[19a]

The formation of oxygen-deficient anatase TiO_2 sheets with dominant (001) facets may be attributed to the synergistic functions of HF and H_2 released from the acid hydrolysis process of TiB_2, which shows a metallic structure and property; the fluorine ions help to stabilize the (001) facet by forming surface Ti−F bonds[8,9] while H_2 reduces the Ti^{4+} on the surface to generate oxygen vacancies.[14,20] In addition, in contrast to the pure H_3BO_3 as the single byproduct recovered from the reaction solution after the hydrolysis of TiB_2 in HCl solution,[14] the byproduct recovered is quite different and complex. Although elemental analysis can confirm the existence of Ti, B, F, and O in the byproduct, the exact identification of its crystal structure is still not reached.

Raman spectra were used to preliminarily investigate the exerted influence of oxygen deficiency on the geometric structure, in particular surface structures of anatase TiO_2 sheets with dominant (001) facets. As shown in Figure 5, the oxygen-deficient TiO_2 sheets show remarkably different Raman-active modes from the reference anatase TiO_2 (Aldrich). Four key features can be revealed by comparing their spectra: The first feature is the unchanged three Raman modes of B_{1g} (397 cm^{-1}), A_{1g} (517 cm^{-1}), and E_g (637 cm^{-1}) in the as-prepared oxygen-deficient sheets. Second, its two E_g modes at 143 and 196 cm^{-1} are shifted by 4 and 13 cm^{-1}, respectively, toward high frequency. Third but more importantly, besides the above five typical Raman modes of anatase TiO_2, two new modes appear at 155 and 171 cm^{-1} as evidenced as peaks 2 and 3 in the right inset in Figure 5A. Furthermore, the new mode at 155 cm^{-1} instead of the E_g mode at 147 cm^{-1} in oxygen-deficient anatase TiO_2 sheets is predominant compared to the reference anatase TiO_2. Interestingly, the two modes at 155 and 171 cm^{-1} completely disappeared after the removal of both oxygen deficiency and surface fluorine from TiO_2 sheets by simply calcining the sample in air. Meanwhile, it is also noted that the E_g mode at 209 cm^{-1} is partially recovered to 200 cm^{-1} (the left inset in Figure 5A), and other modes are unchanged. Finally, it is found that the B_{1g} mode at 397 cm^{-1} is greatly weakened in oxygen-deficient anatase TiO_2 sheets (see Figure 5B, curve b) and can be recovered by the removal of oxygen deficiency and surface fluorine after calcination in air (see Figure 5B, curve c). The fact that the oxygen-deficient TiO_2 sheets have quite different Raman spectra from oxygen-free TiO_2 sheets but the nearly same XRD patterns as oxygen deficiency-free TiO_2 sheets (see Figure 1) suggests that most oxygen deficiency related Ti^{3+} should mainly localize within the surface and subsurface of the sheets.

To understand the origin of the two new active modes and the weakened E_g mode at 397 cm^{-1}, we further compared their Raman spectra of the anatase TiO_2 sheets with and without only surface fluorine from ref 8. As shown in Figure 5C, no any new active mode is generated in only fluorine-terminated anatase TiO_2 sheets, suggesting that the new modes at 155 and 171 cm^{-1} observed in Figure 3a are independent of sole surface fluorine.

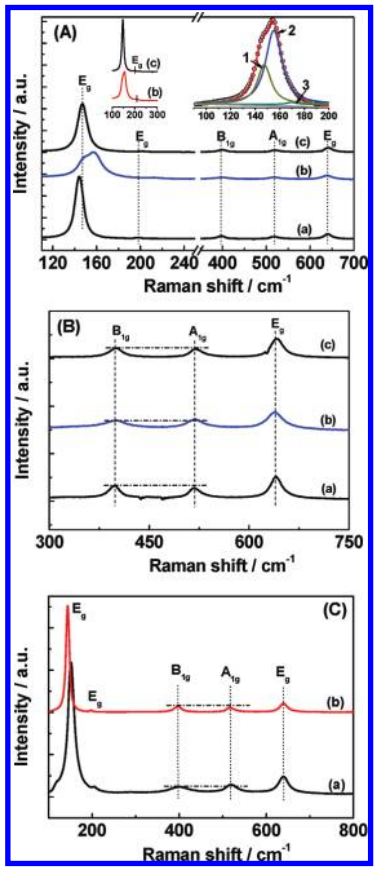

Figure 5. Raman spectra in the ranges of (A) 110−700 cm^{-1} and (B) 300−750 cm^{-1} of the reference anatase TiO_2 (Aldrich, product no. 232033) (a), oxygen-deficient anatase sheets (b), and anatase sheets free of oxygen deficiency (c). The left inset in panel A is the partial Raman spectra of curves b and c between 100 and 300 cm^{-1}, and the right inset is the fitted E_g mode at 100−200 cm^{-1} in curve b. Raman spectra (C) of (a) surface fluorine-terminated anatase TiO_2 sheets and (b) anatase TiO_2 sheets free of fluorine, which were prepared according to ref 8.

In the previous investigation on Raman spectra of TiO_2 with oxygen deficiency, it was found that sole oxygen deficiency can only cause some new weak modes at wavenumbers higher than 300 cm^{-1}.[21] On the basis of these results, it is indicative that the two new modes are the synergistic effects of oxygen deficiency and surface fluorine probably by changing both atomic coordination numbers and bonding length of the Ti−O−Ti network in oxygen-deficient anatase TiO_2 sheets with surface-terminated fluorine. These changes generate some new Raman-active phonons. On the other hand, the similar weakening of the B_{1g} mode at 397 cm^{-1} is also evidenced in Figure 5C, indicating that surface-terminated fluorine is responsible for such weakening by changing the coordination number of surface Ti atoms and thus the vibrational amplitudes of the nearest neighbors. As for the shift of E_g mode at 144−151 cm^{-1} between two samples in Figure 5C, the proposed reason is that the surface-terminated fluorine can change the symmetry of Ti−O−Ti and hence the force constant, which usually causes the wavenumber shift of some modes.[22,23b]

The above results clearly show an important feature that oxygen deficiency in TiO_2 sheets with surface-terminated fluorine results in the remarkable surface reconstruction evidenced by two new Raman modes at 155 and 171 cm^{-1} and the weakened B_{1g} mode at 397 cm^{-1}. In a previous work,[23a,b] B/N codoping was illuminated to be effective in reconstructing photocatalytic active surfaces of anatase TiO_2 nanoparticles by

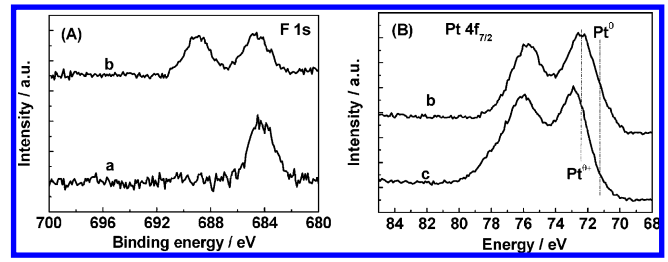

Figure 6. High-resolution XPS spectra of (A) F 1s and (B) Pt 4f for (a) oxygen-deficient anatase TiO_2 sheets, (b) Pt-loaded oxygen-deficient anatase TiO_2 sheets, and (c) Pt-loaded anatase TiO_2 sheets free of oxygen deficiency.

forming Ti−B−N/Ti−O−B−N structure. Recently,[24] the reconstructed surfaces of anatase TiO_2 nanocrystals for efficient photocatalysis, similarly revealed by two new Raman-active modes at 182 and 192 cm^{-1}, were realized by forming surface I−O−Ti bond structure. In both cases, the favorable surface structures facilitating surface separation of charge carriers were constructed by introducing heteroatoms. On the contrary, in the current case of anatase TiO_2 sheets with ca. 44% (101) and 56% (001) facets, the reconstructed surfaces for photocatalysis can be created by the synergistic effects of oxygen deficiency and surface fluorine species. The reconstructed surfaces here are proposed to consist of exposed Ti atoms with lower coordination numbers, i.e., four-coordinated Ti, which may be more favorable sites for reactants in reactions.

We compared the efficiency for hydrogen production of the anatase sheets loaded with 1 wt % Pt species in photochemical reduction of water in the presence of methanol as a scavenger. The oxygen-deficient anatase sheets show a much higher hydrogen evolution rate than the sheets free of oxygen deficiency (2332 vs 1333 $\mu mol \cdot h^{-1} \cdot m^{-2}$). This enhancement can be further understood from the strengthened interaction between Pt-loaded and anatase TiO_2 matrix containing both oxygen deficiency and fluorine via the special electron-transfer process. As shown in Figure 6, it was found that the binding energy of Pt $4f_{7/2}$ (main peak) on oxygen-deficient anatase TiO_2 sheets has a shift by 0.4 eV toward low energy in contrast to that on oxygen deficiency-free anatase TiO_2 sheets. Surprisingly, two unexpected features are evidenced in the F 1s spectra after loading Pt on oxygen-deficient anatase TiO_2 sheets. One is the binding energy shift of original F 1s peak at 684.2−684.6 eV. The other is that a new peak with its center at 690.0 eV appears. The loading of Pt on anatase TiO_2 with surface fluorine can only cause the binding energy shift and no new peak. These results suggest that the energy shift of the original F 1s peak is probably originated from a direct electron transfer from fluorine to Pt on TiO_2 surface containing only fluorine, whereas the new peak may be attributed to an indirect but more efficient electron transfer from fluorine to Pt via adjacent oxygen vacancies on TiO_2 surface containing both oxygen deficiency and fluorine. The latter process can strengthen the interaction between loaded Pt and TiO_2 matrix, which facilitates the transfer of photoinduced electrons from TiO_2 to Pt for more efficient photo water splitting as evidenced.

Equally important, it is interesting to note that the loaded Pt consists of a main portion of $Pt^{\theta+}$ and a small portion of Pt^0. It is generally accepted that only Pt^0 can act as reactive sites for photocatalytic H_2 evolution. However, the formed $Pt^{\theta+}$ species was proposed to play a positive effect on the photocatalytic activity by decreasing the contact resistance at the interface.[25] Further investigation including the deconvolution of Pt 4f spectra and varying the ratio of $Pt^0/Pt^{\theta+}$ will deepen the understanding

SCHEME 1: Proposed Two Pathways of Electron Transferring between Surface Fluorine Atoms and Pt Consisted of $Pt^0/Pt^{\theta+}$ Loaded on Two Different Anatase TiO_2 Surface Sites[a]

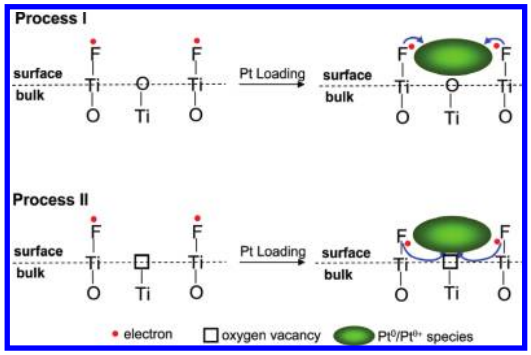

[a] Process I proposes the direct electron transfer from fluorine to Pt consisting of $Pt^0/Pt^{\theta+}$, and process II gives the indirect electron transfer from fluorine to Pt consisting of $Pt^0/Pt^{\theta+}$ via oxygen vacancies. For simplicity, the coordination numbers of surface Ti and O atoms are not considered here.

of Pt cocatalyst. The above ideas proposed have been summarized as Scheme 1.

4. Conclusions

Oxygen-deficient anatase TiO_2 sheets with dominant reactive (001) facets were prepared by using crystalline TiB_2 as an alternative titanium source. Oxygen deficiency and surface fluorine species can trigger obvious surface reconstruction of TiO_2 sheets. Importantly, such reconstruction can strengthen the interaction between Pt-loaded and TiO_2 matrix via a special electron-transfer process involving oxygen vacancies. As a result of both the surface reconstruction and the strengthened interaction, these oxygen-deficient TiO_2 sheets with loaded Pt shows substantially enhanced photoactivity in hydrogen evolution in contrast to TiO_2 sheets free of oxygen deficiency. This material is expected to have attractive applications in dye-sensitized solar cells, photocatalysis, optoelectronic devices, and sensors.

Acknowledgment. The financial support from the Major Basic Research Program, Ministry of Science and Technology of China (No. 2009CB220001), NSFC (No. 50921004), the KJCX2-YW-H21-01, and the Solar Energy Program of the Chinese Academy of Sciences, the IMR SYNL-T.S. Kê Research Fellowship, the Australian Research Council through its Centre's Grant and DP0666345, and Pujiang Talents Program of Science and Technology Commission of Shanghai Municipality (09PJ1402800) is gratefully acknowledged.

References and Notes

(1) Hoffmann, M. R.; Martin, S. T.; Choi, W.; Bahnemann, D. W. *Chem. Rev.* **1995**, *95*, 69–96.

(2) Linsebigler, A. L.; Lu, G. Q., Jr.; Yates, J. T. *Chem. Rev.* **1995**, *95*, 735–758.

(3) (a) Chen, X.; Mao, S. S. *Chem. Rev.* **2007**, *107*, 2891–2959. (b) Liu, G.; Wang, L. Z.; Yang, H. G.; Cheng, H. M.; Lu, G. Q. *J. Mater. Chem.* [Online early access]. DOI 10.1039/B909930A. Published Online: September 18, **2009**. http://www.rsc.org/Publishing/Journals/JM/article.asp?doi=b909930a.

(4) (a) Tada, H.; Mitsui, T.; Kiyonaga, T.; Akita, T.; Tanaka, K. *Nat. Mater.* **2006**, *5*, 782–786. (b) Sakthivel, S.; Kisch, H. *Angew. Chem., Int. Ed.* **2003**, *42*, 4908–4911. (c) Li, J.; Zeng, H. C. *Angew. Chem., Int. Ed.* **2005**, *44*, 4342–4345. (d) Jiang, C. H.; Wei, M. D.; Qi, Z. M.; Kudo, T.; Honma, I.; Zhou, H. S. *J. Power Sources* **2007**, *166*, 239–243. (e) Qi, Z. M.; Honma, I.; Zhou, H. S. *J. Phys. Chem. B* **2006**, *110*, 10590–10594.

(5) Schattka, J. H.; Shchukin, D. G.; Jia, J. G.; Antonietti, M.; Caruso, R. A. *Chem. Mater.* **2002**, *14*, 5103–5108.

(6) Wen, W.; Zhao, H. J.; Zhang, S. Q.; Pires, V. *J. Phys. Chem. C* **2008**, *112*, 3875–3880.

(7) Selloni, A. *Nat. Mater.* **2008**, *7*, 613–615.

(8) Yang, H. G.; Sun, C. H.; Qiao, S. Z.; Zou, J.; Liu, G.; Smith, S. C.; Cheng, H. M.; Lu, G. Q. *Nature* **2008**, *453*, 638–641.

(9) Yang, H. G.; Liu, G.; Qiao, S. Z.; Sun, C. H.; Jin, Y. G.; Smith, S. C.; Zou, J.; Cheng, H. M.; Lu, G. Q. *J. Am. Chem. Soc.* **2009**, *131*, 4078–4083.

(10) (a) Wu, B. H.; Guo, C. Y.; Zheng, N. F.; Xie, Z. X.; Stucky, G. D. *J. Am. Chem. Soc.* **2008**, *130*, 17563–17567. (b) Han, X. G.; Kuang, Q.; Jin, M. S.; Xie, Z. X.; Zheng, L. S. *J. Am. Chem. Soc.* **2009**, *131*, 3152–3153. (c) Dai, Y. Q.; Cobley, C. M.; Zeng, J.; Sun, Y. M.; Xia, Y. N. *Nano Lett.* **2009**, *9*, 2455–2459. (d) Amano, F.; Yasumoto, T.; Prieto-Mahaney, O. O.; Uchida, S.; Shibayama, T.; Ohtani, B. *Chem. Commun.* **2009**, 2311–2313. (e) Zhang, D. Q.; Li, G. S.; Yang, X. F.; Yu, J. C. *Chem. Commun.* **2009**, 4381–4383. (f) Amano, F.; Prieto-Mahaney, O. O.; Terada, Y.; Yasumoto, T.; Shibayama, T.; Ohtani, B. *Chem. Mater.* **2009**, *21*, 2601–2603. (g) Alivov, Y.; Fan, Z. Y. *J. Phys. Chem. C* **2009**, *113*, 12954–12957. (h) Liu, G.; Yang, H. G.; Wang, X. W.; Cheng, L.; Pan, J.; Lu, G. Q.; Cheng, H. M. *J. Am. Chem. Soc.* **2009**, *131*, 12868–12869.

(11) Nakamura, I.; Negishi, N.; Kutsuna, S.; Ihara, T.; Sugihara, S.; Takeuchi, K. *J. Mol. Catal. A: Chem.* **2000**, *161*, 205–212.

(12) Justicia, I.; Ordejon, P.; Canto, G.; Mozos, J. L.; Fraxedas, J.; Battiston, G. A.; Gerbasi, R.; Figueras, A. *Adv. Mater.* **2002**, *14*, 1399–1402.

(13) Gong, X. Q.; Selloni, A.; Batzill, M.; Diebold, U. *Nat. Mater.* **2006**, *5*, 665–670.

(14) Liu, G.; Yang, H. G.; Sun, C. H.; Cheng, L. N.; Wang, L. Z.; Lu, G. Q.; Cheng, H. M. *CrystEngComm* **2009**, *11*, 2677 DOI: 10.1039/b909191m.

(15) Wang, X. W.; Liu, G.; Chen, Z. G.; Li, F.; Wang, L. Z.; Lu, G. Q.; Cheng, H. M. *Chem. Commun.* **2009**, 3452.

(16) Munro, R. G. *J. Res. Natl. Inst. Stand. Technol.* **2000**, *105*, 709–720.

(17) (a) Thompson, T. L., Jr.; Yates, J. T. *Chem. Rev.* **2006**, *106*, 4428–4453. (b) Lin, Z.; Orlov, A.; Lambert, R. M.; Payne, M. C. *J. Phys. Chem. B* **2005**, *209*, 20948–20952.

(18) (a) Yu, J. C.; Yu, J.; Ho, W.; Jiang, Z.; Zhang, L. *Chem. Mater.* **2002**, *14*, 3808–3816. (b) Zhou, J. K.; Lv, L.; Yu, J. Q.; Li, H. L.; Guo, P. Z.; Sun, H.; Zhao, X. S. *J. Phys. Chem. C* **2008**, *112*, 5316–5321.

(19) (a) Batzill, M.; Morales, E. H.; Diebold, U. *Chem. Phys.* **2007**, *339*, 36–43. (b) Czoska, A. M.; Livraghi, S.; Chiesa, M.; Giamello, E.; Agnoli, S.; Granozzi, G.; Finazzi, E.; Di Valentin, C.; Pacchioni, G. *J. Phys. Chem. C* **2008**, *112*, 8951–8956.

(20) Greenwood, N. N.; Parish, R. V.; Thornton, P. *Q. Rev., Chem. Soc.* **1966**, *20*, 441–464.

(21) Liu, G.; Li, F.; Wang, D. W.; Tang, D. M.; Liu, C.; Ma, X. L.; Lu, G. Q.; Cheng, H. M. *Nanotechnology* **2009**, *19*, 025606.

(22) Liu, G.; Chen, Z. G.; Dong, C. L.; Zhao, Y. N.; Li, F.; Lu, G. Q.; Cheng, H. M. *J. Phys. Chem. B* **2006**, *110*, 20823–20828.

(23) (a) Liu, G.; Zhao, Y. N.; Sun, C. H.; Li, F.; Lu, G. Q.; Cheng, H. M. *Angew. Chem., Int. Ed.* **2008**, *47*, 4516–4520. (b) Liu, G.; Sun, C. H.; Cheng, L. N.; Jin, Y. G.; Lu, H. F.; Wang, L. Z.; Smith, S. C.; Lu, G. Q.; Cheng, H. M. *J. Phys. Chem. C* **2009**, *113*, 12317–12324.

(24) Liu, G.; Sun, C. H.; Yan, X. X.; Cheng, L. N.; Chen, Z. G.; Wang, X. W.; Wang, L. Z.; Smith, S. C.; Lu, G. Q.; Cheng, H. M. *J. Mater. Chem.* **2009**, *19*, 2822–2829.

(25) Li, Q. Y.; Wang, K.; Zhang, S. L.; Zhang, M.; Yang, J. J.; Jin, Z. S. *J. Mol. Catal. A: Chem.* **2006**, *258*, 83.

JP907749R